Aerosol and Air Quality Research, 9: 453-457, 2009

ISSN: 1680-8584 print / 2071-1409 online
doi: 10.4209/aaqr.2009.05.0033

First Differential Mobility Analysis (DMA) Measurements of Air Ions Produced by Radioactive Source and Corona

Manuel Alonso[1], José P. Santos[2], Esther Hontañón[2*], Emilio Ramiro[2]

[1] *National Centre for Metallurgical Research (CSIC), Avenida Gregorio del Amo 8, 28040 Madrid, Spain*
[2] *RAMEM S.A., Sambara 33, 28027 Madrid, Spain*

ABSTRACT

A recently developed Differential Mobility Analyzer (DMA) of high resolving power (50 for ions of mobility equivalent diameter~1 nm) has been used to measure the mobility distribution of laboratory air ions generated by ^{241}Am and corona discharge. In the case of ^{241}Am, it has been possible to follow the changes in mobility during the early stages of ion aging: within the time interval between 10 and 30 ms after ion formation, the mean reduced mobility of positive ions decreased from 1.30 to 1.15 cm^2/Vs, and that of negative ions from 2.0 to 1.75 cm^2/Vs. The mobility distribution of air ions at the outlet of a corona ionizer strongly depends on the corona voltage, mainly due to the mobility-dependent extent of electrostatic losses within the ionizer. The mean reduced mobility of corona ions ranged between 1.01 and 1.20 cm^2/Vs (positive) and 1.76 and 1.96 cm^2/Vs (negative).

Keywords: Differential mobility analyzer; Resolution; Ion aging; Radioactive source; Corona discharge.

INTRODUCTION

Particle charging is a process of great importance to the field of aerosol science and technology. Indoor air cleaners, industrial electrostatic precipitators, and smoke detectors are instances of practical apparatuses and instruments which ultimately rely upon the capability of airborne particles to acquire a net electric charge. A different kind of application of particle charging is found in the measurement of the particle size distribution of submicron aerosols by differential mobility analysis. For the latter, one must be able to produce a known and stable charge distribution on the particles (Flagan, 2001).

In practice, particle charging is usually carried out by making the aerosol to flow through a region where ions are being continuously generated, generally by a radioactive source or by an electric discharge, from the molecules of the gas where the particles are suspended. The thus generated ions move towards the particles, either by diffusion (diffusion charging) or following the electric field lines in the case that an external electric field is being applied (field charging) (Liu and Kapadia, 1978). Upon collision with particles, ions get attached to their surface. Actually, the mechanism of diffusion charging is always at work, even if there is an external electric field, especially in the case of ultrafine aerosol particles (Alguacil and Alonso, 2006).

According to the currently accepted theories of diffusion charging (Fuchs, 1963; Hoppel and Frick, 1986), the rate at which particles acquire charges depends basically on the particle size, the number and polarity of the charges on the particle, and the physical properties of ions, such as the mean free path, the mean thermal velocity and the diffusion coefficient. All these properties can be estimated upon knowledge of just two ionic properties: mass and mobility.

Ion mobility has not been measured in practically any of the past works on aerosol charging, except for a few cases. Ion mass has not been measured in any of those works. The traditional approach has consisted in selecting appropriate values for the ionic mass and mobility so as to match the experimental results with the diffusion charging theory of Fuchs (or its later modifications). As a result, the values of ion mass and mobility reported in the aerosol charging literature lie within a considerable wide range of values, in spite that in most of the works the ion generation technique employed was the same, e.g. air ions generated from ^{241}Am (Hussin *et al.*, 1983; Wen *et al.*, 1984; Adachi *et al.*, 1985; Hoppel and Frick, 1986; Wiedensohler *et al.*, 1986; Hoppel and Frick, 1990; Wiedensohler and Fissan, 1991; Alonso *et al.*, 1997).

The chemical nature of the air ions is rather complex, depending basically on the nature of trace gases and contaminants present in the air, on the water content of air as well as on the age of the ions. The mass spectra of negative ions produced by α rays in artificial air at atmospheric pressure have been measured (Cabane and Playe, 1980). They observed two main categories of ions: hydrates built on simple ions, such as $O_2^-(H_2O)_n$, $O_3^-(H_2O)_n$, $OH^-(H_2O)_n$, $CO_3^-(H_2O)_n$, $CO_4^-(H_2O)_n$, $NO_2^-(H_2O)_n$, $NO_3^-(H_2O)_n$, etc., and hydrates of complex ions such as $NO_x^-HNO_y(H_2O)_n$, $HCO_3^-HNO_y(H_2O)_n$, and the like. On their part, the most abundant positive air ions are also hydrates of the type $(H_3O)^+(H_2O)_n$, $O_2^+(H_2O)_n$, $NO^+(H_2O)_n$ and $NO_2^+(H_2O)_n$ (Huertas *et al.*, 1971).

A real assessment of Fuchs diffusion charging theory requires precise knowledge of ion mass and mobility. In the present work, we present the results of experimental measurements of mobility distributions of laboratory air ions generated by ^{241}Am and corona discharge, which are among the typical ions usually employed in aerosol charging studies. For the measurements, we have used a recently developed differential mobility analyzer (DMA) capable of high-resolution measurement of mobility in the range 0.5-3.0 cm^2/Vs.

METHODS

The Planar Differential Mobility Analyzer

* Corresponding author. Tel: 34-91-404-4575;
Fax: 34-91-403-4596
E-mail address: e.hontanon@ramem.com

Mobility measurements were carried out using a parallel-plate DMA (IONER X1, RAMEM, Madrid, Spain), a brief description of which is made in the following; the details can be found elsewhere (Ramiro and Rivero, 2007; Santos *et al.*, 2009). A schematic of a parallel-plate DMA is depicted in Fig. 1. The core of the DMA is the classification region, where an electric field is established perpendicularly to a gas flow (sheath flow). Ions entering the classification region through the inlet slit moves under the influence of both electric field and sheath flow. Ideally this flow is uniform (plug flow) and the electric field between the parallel planar electrodes is uniform also. Under these conditions, only the ions of a mobility given by

$$Z = \frac{Q}{V}\frac{\Delta_y}{\Delta_x \Delta_z} \quad (1)$$

exit the DMA through the outlet slit. In Eq. (1), Q is the sheath flow rate, V is the potential difference between the electrodes, Δ_y is the separation between the electrodes (5 mm), Δ_x is the distance between the ion inlet and outlet slits (5 mm), and Δ_z is the width of the classification zone (10 mm).

The parallel-plate electrodes are inserted within a closed-circuit rectangular duct in which the sheath gas, usually air, flows at Reynolds numbers between 20.000 and 90.000 (corresponding to flow rates of 200 to 900 L/min). Transition to turbulence could be avoided by using three stages of laminarizing screens. The classified ions were detected with an electrometer (IONER EL5010, RAMEM, Madrid, Spain) having a noise level of the order of 0.1 fA RMS. To prevent buildup of unclassified ions in the recirculation loop, a small-scale electrostatic precipitator was inserted within the loop, downstream of the classification zone. The sheath gas loop circuit is also equipped with a Venturi-type flowmeter (model V-Cone, McCrometer, CA, USA) and with pressure and temperature sensors, all placed upstream of the classification region. The actual sheath flow rate in the classification zone is calculated from the upstream measured flow rate, pressure and temperature, assuming isentropic flow conditions.

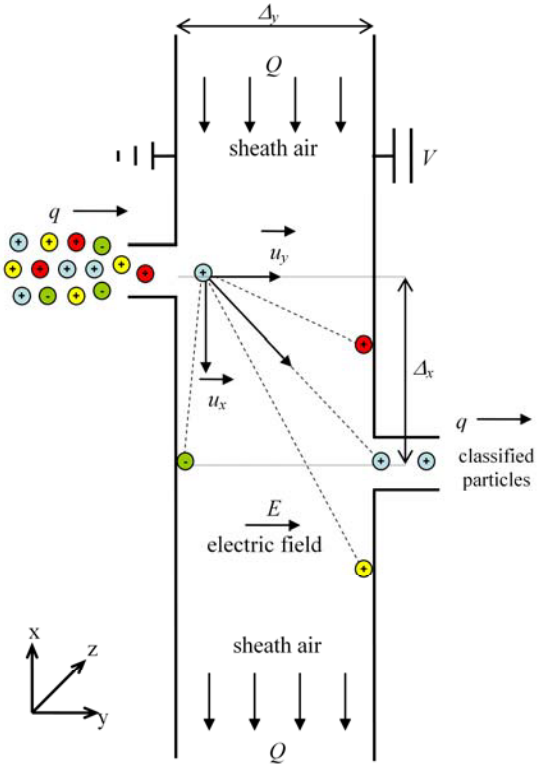

Fig. 1. Sketch of a parallel-plate DMA.

Air Ions Generated by ^{241}Am

Room air was pumped through a packed bed of silica gel and an absolute filter. Ions were generated by passing this clean dry air through a radioactive ionizer, a sketch of which is shown in Fig. 2(a). It consists of a circular copper tube, 2 cm long and 4 mm ID, containing two thin disks (ϕ 5 mm) of ^{241}Am near its outlet end, each with a nominal activity of 0.9 μCi. The radioactive source disks were placed in the inner wall of the tube at two diametrically opposite positions. The outlet of the ionizer was directly connected to the inlet tube of the DMA. For a given flow rate of air through the ionizer, the volume between the ^{241}Am disks and the DMA inlet slit, 1.04 cm^3, was used to estimate the age of the ions fed to the DMA. Experiments were performed with air flow rates through the ionizer (equal to the ion flow rate into the DMA) between 2 and 6 L/min. The sheath air flow rate was kept constant at 350 L/min (as measured upstream of the classification zone).

Air Ions Generated by Corona Discharge

For this series of experiments, clean dry room air, prepared as described in the preceding section, was pumped into a laboratory-made corona discharge ionizer, which is displayed in Fig. 2(b). The latter consisted of a cylinder made of brass (18 mm ID, 15 mm in length), a coaxial stainless steel needle electrode connected to a high-voltage supply, and a stainless steel grounded electrode plate attached to the cylinder outlet and having a 4 mm circular orifice at its center. For the experiments, different voltages (and polarity) were applied between the needle and the rear plate, keeping constant the air flow rate through the ionizer at 3 L/min. In another series of experiments, the applied voltage was fixed at -1.7 kV and the air flow rate was varied between 2 and 4 L/min. The DMA sheath flow rate was kept constant at 350 L/min (as measured with the Venturi-type flowmeter) in all the experiments.

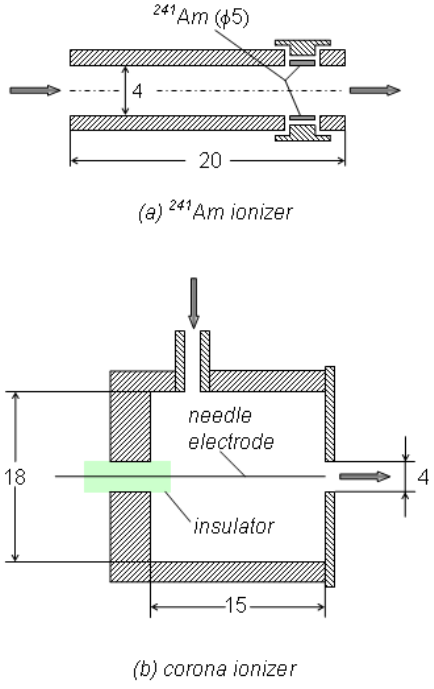

Fig. 2. Layout of the radioactive ionizer of ^{241}Am (top) and of the corona discharge ionizer (bottom) used in this work.

RESULTS AND DISCUSSION

All the mobility spectra reported below were normalized so that the area under each spectrum is unity. In this manner, the relative intensity of each peak represents the relative abundance of the corresponding ion in the mixture. In all the spectra, the x-axis represents the reduced mobility, Z_0, calculated at 0ºC and atmospheric pressure using the Langevin's expression

$$Z_0 = Z\left(\frac{P}{760}\right)\left(\frac{273}{T}\right) \quad (2)$$

where Z is the mobility measured at the conditions of pressure P (mmHg) and absolute temperature T (K) prevailing at the classification zone of the DMA.

Air Ions from ^{241}Am

Fig. 3 shows the effect of aging time on the mobility spectra of negative air ions generated by ^{241}Am. As previously explained, aging times were estimated as the mean residence time spent by ions in the way between the radioactive source disks and the inlet slit of the DMA. The estimated aging times ranged between 0.01 and 0.03 s; thus, the studied ions are almost newly formed, unaged ions. We could not measure the mobility of ions with age above, let's say, 0.1 s, because for this we had to use a relatively long tube connecting the ionizer and the DMA, resulting in rather high losses by diffusion and electrostatic dispersion and, consequently, very low currents (slightly above the electrometer noise level) at the sampling stream of the DMA.

Although the differences in the spectra shown in Fig. 3 are not so pronounced, it can nevertheless be noticed an effect of the aging time on ion mobility. Ions grow progressively by chemical reactions and clustering processes. The air passing through the ionizer was filtered and dried, but it certainly contained water molecules even if in trace amounts. The main peak, at reduced mobility around 2 cm^2/Vs, is presumably a mixture of several ionic species differing in the number of clustered water molecules; these ions grow in time by attachment of further water molecules. The result is that the peaks shift toward lower mobility (i.e., larger ion size) with aging time.

The same general trend can be observed in Fig. 4, where the mobility distribution of positive ions generated by the ^{241}Am source is shown as a function of the ion aging time. The spectrum of positive ions is much more complex than that of negative air ions and, in fact, it appears as a sort of continuous distribution of mobility between around 0.7 and 2.2 cm^2/Vs. The effect of aging can be more clearly observed for the peak of highest mobility (~2 cm^2/Vs), which undergoes a considerable shift toward lower mobility with time. As noted before, the normalization of the spectra permits visualization of the general trend: older ions show higher relative peak intensities in the lower region of the mobility spectrum.

The results shown in Figs. 3 and 4 are coherent with the findings of Nagato and Ogawa (1998) employing an ion mobility spectrometer with a drift tube to measure the mobility of air ions aged for about 0.03-5 s; they found six main mobility peaks, between 1.0 and 2.0 cm^2/Vs, for positive ions, and two peaks at mobilities 1.7 and 1.9 cm^2/Vs for negative ions.

The general tendency of the effect of aging time on ion mobility can perhaps be more readily observed in Fig. 5, which shows the mean mobility of positive and negative air ions generated by ^{241}Am as a function of time for the very early stages of the aging process. Note, for instance, that the mean mobility of negative ions decays from almost 2.0 cm^2/Vs to 1.75 cm^2/Vs in just 20 ms, and that of positive ions from 1.3 to 1.15 cm^2/Vs. This may explain the large scattering of mobility values employed by different authors in past aerosol charging studies, which are shown in Table 1. As mentioned before, these mobility values were, in most instances, chosen so as to match the predictions of Fuchs' diffusion charging theory with the

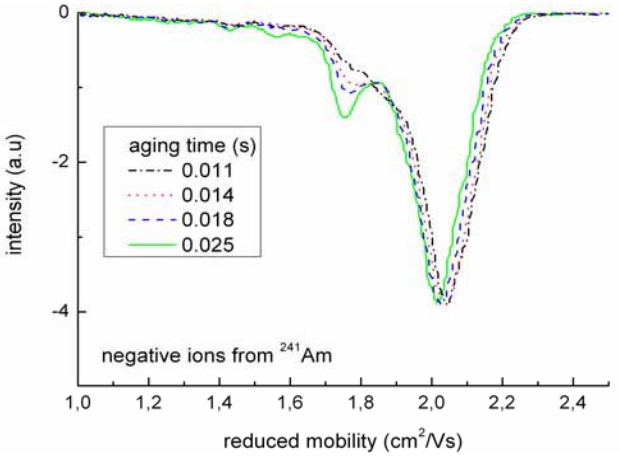

Fig. 3. Evolution of the mobility distribution of negative air ions generated by ^{241}Am during the early stages of aging.

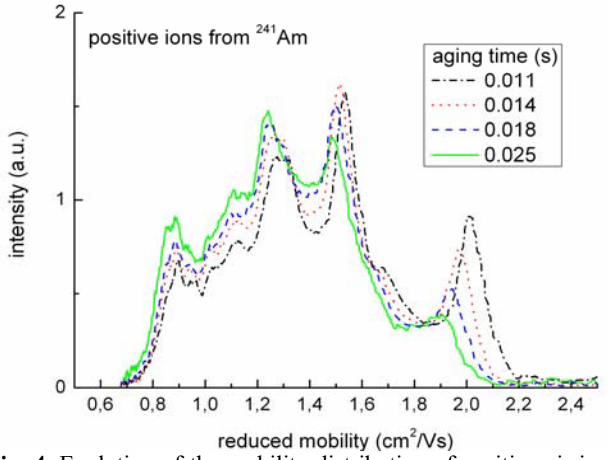

Fig. 4. Evolution of the mobility distribution of positive air ions generated by ^{241}Am during the early stages of aging.

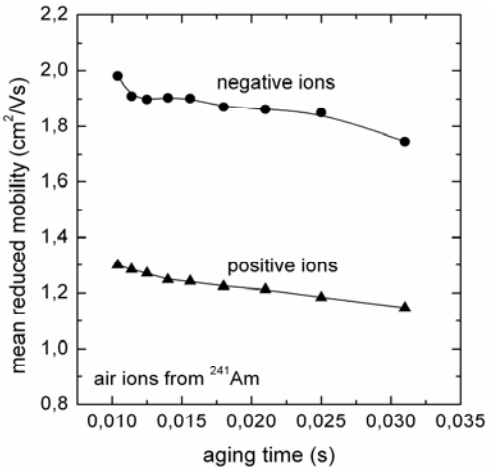

Fig. 5. Time evolution of the mean mobility during the first stages of the aging process for ions generated by ^{241}Am.

Table 1. Values of ion mobility used in particle charging studies.

Authors	Z^+ (cm^2/Vs)	Z^- (cm^2/Vs)
Hussin *et al.* (1983)	1.15	1.39
Wen *et al.* (1984) and Adachi *et al.* (1986)	1.40	1.90
Hoppel and Frick (1986)	1.20	1.35
Wiedensohler *et al.* (1986)	1.35	1.60
Hoppel and Frick (1990)	1.33	1.84
Wiedensohler and Fissan (1991)	1.40	1.60
Reischl *et al.* (1996)	1.15	1.43
Alonso *et al.* (1997)	1.15	1.65

experimental results. While the mobilities of positive ions listed in Table 1 are all coherent with the measurements done in the present work, mobilities for negative ions as low as 1.35, 1.39 or 1.43 cm^2/Vs, which have been adopted in some past works, are not reasonable at all.

It is important to recall that the mobilities reported in the above three plots (as well as in the remaining Figures below) are reduced mobilities. The value of mobility at other P, T conditions can be estimated with Langevin's equation, Eq. (2). For example, to estimate the mobility at 20ºC and 1 atm, the reduced mobility should be multiplied by the factor 293/273 = 1.07.

Air Ions from Corona Discharge

The mobility distributions of negative and positive air ions generated by corona discharge are shown, respectively, in Figs. 6 and 7, for different corona voltages. All these spectra were measured at a fixed flow rate of air through the ionizer of 3 L/min, which resulted in a mean residence time of ions of roughly 20 ms between the corona needle tip and the inlet slit of the DMA. Regardless the ion polarity, it can be observed a shift toward lower mobility as the corona voltage is increased. This is a consequence of increasing ion losses by electrostatic precipitation within the corona device. Particularly, in the case of positive ions it can be noticed a remarkable increase in the relative abundance of 0.90 and 0.83 cm^2/Vs ions at high corona field strength, at the expense, of course, of a reduction in the relative proportion of higher mobility ions. In general, varying the corona voltage does not seem to yield any new chemical species.

The effect of corona voltage on the mass of negative air ions generated by corona discharge has been already discussed (Sekimoto and Takayama, 2007). The general trend of their results showed a global shift to larger ion mass as the corona voltage was increased. This is in qualitative agreement with the increase in the relative abundance of lower mobility ions observed in Fig. 7.

The mean air ion mobility as a function of the applied voltage is shown in Fig. 8. In both cases, the mean mobility changes within about 0.2 cm^2/Vs (from 1.01 to 1.20 cm^2/Vs for positive ions, and from 1.76 to 1.96 cm^2/Vs for negative ions).

We also tried to examine the effect of aging time on the mobility distribution of corona ions. However, in this case it is not as clear as for the ions generated by ^{241}Am because, as we have just seen, the mobility distribution itself of the corona ions strongly depends on the applied voltage and, on the other hand, electrostatic losses of ions inside the corona ionizer depend on the applied voltage as well as on the mean residence time of ions inside the ionizer. Therefore, varying the flow rate of air through the ionizer is not an appropriate means to study the effect of ion aging alone. Nevertheless, we carried out a series of measurements keeping constant the corona voltage and varying the flow rate of air through the ionizer. The results, shown in Fig. 9, indicate a global shift toward lower mobility as the air flow decreases. But this is presumably more related to the effect of mobility-dependent electrostatic losses inside the ionizer, rather than to the aging effect.

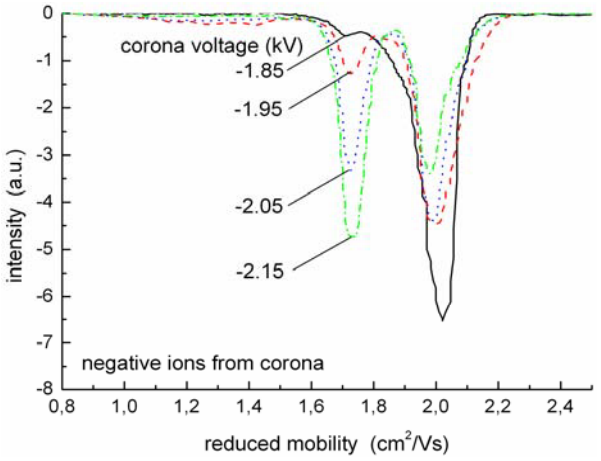

Fig. 6. Mobility spectra of negative air ions as a function of the corona voltage.

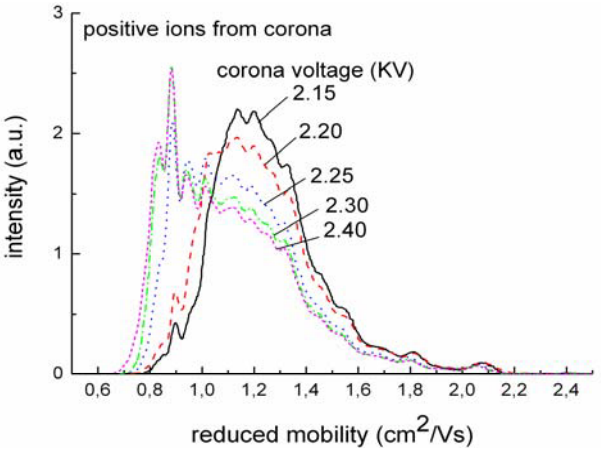

Fig. 7. Mobility spectra of positive air ions as a function of the corona voltage.

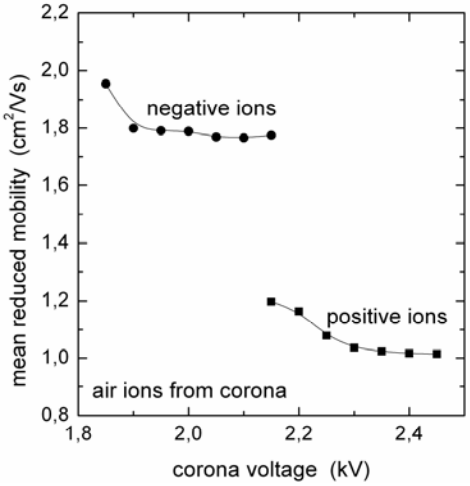

Fig. 8. Mean mobility of air ions generated by corona discharge as a function of the corona voltage.

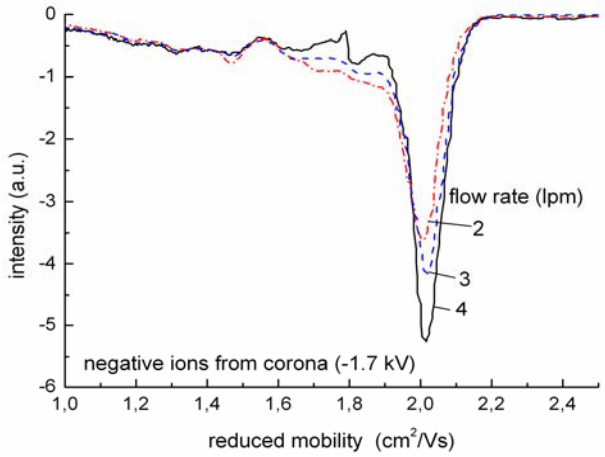

Fig. 9. Effect of air flow rate on the mobility distribution of ions generated by corona discharge.

CONCLUSIONS

The mobility distribution of typical laboratory air ions employed in aerosol charging studies has been measured. Specifically, we have measured the mobility of air ions generated by ^{241}Am and its evolution during the very early stages of the aging process, as well as the mobility spectra of ions generated by corona discharge as a function of the applied voltage and polarity. In general, the mobility distribution of air ions strongly depends on their age and, in the case of ions generated by corona, on the extent of electrostatic losses within the ionizer. The large scattering of mobility values employed by different authors in past aerosol charging studies is coherent with the experimental findings of the present study.

REFERENCES

Adachi, M., Kousaka, Y. and Okuyama, K. (1986). Unipolar and Bipolar Diffusion Charging of Ultrafine Aerosol Particles. *J. Aerosol Sci*. 16: 109-123.

Alguacil, F.J. and Alonso, M. (2006). Multiple Charging of Ultrafine Particles in a Corona Charger. *J. Aerosol Sci*. 37: 875-884.

Alonso, M., Kousaka, Y., Nomura, T., Hashimoto, N. and Hashimoto, T. (1997). Bipolar Charging and Neutralization of Nanometer-Sized Aerosol Particles. *J. Aerosol Sci.* 28: 1479-1490.

Cabane, M. and Playe, P. (1980). Mass Spectra of Negative Ions in Air-Like Gas Mixtures at Atmospheric Pressure. *J. Aerosol Sci*. 11: 475-482.

Flagan, R.C. (2001). Electrical Techniques, in *Aerosol Measurement: Principles, Techniques, and Applications*, Baron, P.A. and Willeke, K. (Eds.), Wiley-Interscience, New York, p. 537.

Fuchs, N.A. (1963). On the Stationary Charge Distribution on Aerosol Particles in a Bipolar Ionic Atmosphere. *Pure Appl. Geophys.* 56: 185-193.

Hoppel, W.A. and Frick, G.M. (1986). Ion Attachment Coefficients and the Steady State Charge Distribution on Aerosols in a Bipolar Ion Environment. *Aerosol Sci. Technol*. 5: 1-21.

Hoppel, W.A. and Frick, G.M. (1990). The Nonequilibrium Character of the Aerosol Charge Distributions Produced by Neutralizers. *Aerosol Sci. Technol*. 12: 471-496.

Huertas, M.L., Marty, A.M., Fontan, J., Alet, I. and Duffa, G. (1971). Measurement of Mobility and Mass of Atmospheric Ions. *J. Aerosol Sci*. 2: 145-150.

Hussin, A., Scheibel, H.G., Becker, K.H., and Porstendorfer, J. (1983). Bipolar Diffusion Charging of Aerosol Particles – I. Experimental Results within the Diameter Range 4-30 nm. *J. Aerosol Sci*. 14: 671-677.

Liu, B.Y. H. and Kapadia, A. (1978). Combined Field and Diffusion Charging of Aerosol Particles in the Continuum Regime. *J. Aerosol Sci*. 9: 227-242.

Nagato, K. and Ogawa, T. (1998). Evolution of Tropospheric Ions Observed by an Ion Mobility Spectrometer with a Drift Tube. *J. Geophys. Res.* 103: 13917-13925.

Ramiro, E. and Rivero, A. (2007). Wide Range Differential Mobility Analyzer with Very High Resolution. International Patent WO 2007/020303.

Reischl, G.P., Mäkelä, J.M., Karch, R. and Necid, J. (1996). Bipolar Charging of Ultrafine Particles in the Size Range below 10 nm. *J. Aerosol Sci.* 27: 931-949.

Santos, J.P., Hontañón, E., Ramiro, E. and Alonso, M. (2009). Performance Evaluation of a High-Resolution Parallel-Plate Differential Mobility Analyzer. *Atmos. Chem. Phys.* 9: 2419-2429.

Sekimoto, K. and Takayama, M. (2007). Influence of Needle Voltage on the Formation of Negative Core Ions Using Atmospheric Pressure Corona Discharge in Air. *Int. J. Mass Spectrom.* 261: 38-44.

Wen, H.Y., Reischl, G.P., and Kasper, G. (1984). Bipolar Diffusion Charging of Fibrous Aerosol Particles. *J. Aerosol Sci.* 15: 89-122.

Wiedensohler, A., Lutkenmeier, E., Feldpausch, M. and Helsper, C. (1986). Investigation of the Bipolar Charge Distribution at Various Gas Conditions. *J. Aerosol Sci.* 17: 413-416.

Wiedensohler, A. and Fissan, H.J. (1991). Bipolar Charge Distributions of Aerosol Particles in High-Purity Argon and Nitrogen. *Aerosol Sci. Technol.* 14: 358-364.

Received for review, May 19, 2009
Accepted, June 27, 2009